

Spatiotemporal modelling of PM_{2.5} concentrations in Lombardy (Italy) – A comparative study

Philipp Otto
University of Glasgow

Alessandro Fusta Moro
University of Bergamo

Jacopo Rodeschini
University of Bergamo

Qendrim Shaboviq
Leibniz University Hannover

Rosaria Ignaccolo
University of Turin

Natalia Golini
University of Turin

Michela Cameletti
University of Bergamo

Paolo Maranzano
University of Milan-Bicocca, Fondazione Eni Enrico Mattei (FEEM)

Francesco Finazzi
University of Bergamo

Alessandro Fassò
University of Bergamo

September 15, 2023

Abstract

This study presents a comparative analysis of three predictive models with an increasing degree of flexibility: hidden dynamic geostatistical models (HDGM), generalised additive mixed models (GAMM), and the random forest spatiotemporal kriging models (RFSTK). These models are evaluated for their effectiveness in predicting PM_{2.5} concentrations in Lombardy (North Italy) from 2016 to 2020. Despite differing methodologies, all models demonstrate proficient capture of spatiotemporal patterns within air pollution data with similar out-of-sample performance. Furthermore, the study delves into station-specific analyses, revealing variable model performance contingent on localised conditions. Model interpretation, facilitated by parametric coefficient analysis and partial dependence plots, unveils consistent associations between predictor variables and PM_{2.5} concentrations. Despite nuanced variations in modelling spatiotemporal correlations, all models effectively accounted for the underlying dependence. In summary, this study underscores the efficacy of conventional techniques in modelling correlated spatiotemporal data, concurrently highlighting the complementary potential of Machine Learning and classical statistical approaches.

Keywords: Air pollution, spatiotemporal process, geostatistics, machine learning, hidden dynamic geostatistical model, generalised additive mixed model, random forest spatiotemporal kriging.

1 Introduction

The Lombardy region, situated in the heart of the Po Valley in Northern Italy, is known to be highly polluted due to the natural barrier created by the Alps hindering the dispersion of air pollutants (see, e.g., Pernigotti et al., 2012). Fine particulate matter (PM_{2.5}) has been identified as the most hazardous air pollutant (European Environmental Agency, 2022a), representing a mix of air pollutants with a diameter less than 2.5 μ m (see also Jerrett et al., 2005, for a review). Information about the air quality dynamics is essential for decision-makers to effectively mitigate adverse effects. Statistical and machine learning models can offer valuable insights into this behaviour and its consequences, including the identification of pollution sources and the factors influencing its behaviour and forecasting future pollution levels under various scenarios, such as changes in emissions or weather patterns. Moreover, the combination of different modelling techniques may further enhance the results. By leveraging the strengths of each approach, decision-makers can gain a more comprehensive understanding of air pollution and make more informed choices for mitigation strategies.

This paper compares three statistical and machine learning models with varying degrees of flexibility to elucidate daily PM_{2.5} concentrations in the Lombardy region. More precisely, hidden dynamic geostatistical models (HDGM), generalised additive mixed models (GAMM), and random forest spatiotemporal kriging (RFSTK) were utilised to describe the relationships between a large set of predictors and PM_{2.5} concentrations. All three models employed in this study have been specifically developed to handle spatiotemporal data. HDGM incorporates a latent variable to capture spatiotemporal dependence, while external factors are included in a linear manner within the model. Conversely, GAMM allows for the nonlinear impact of exogenous predictors, which are estimated using splines. It incorporates spatiotemporal dependence by utilising a smoothing spline for spatial variation and a first-order autoregressive process for temporal dependence. Lastly, RFSTK employs a random forest (RF) to model the nonlinear effects of predictors and then a spatiotemporal kriging model to account for the possible spatiotemporal dependence.

These models are frequently applied in diverse areas. First, HDGM has been primarily used for air pollution studies (see, e.g., Najafabadi et al. 2020; Taghavi-Shahri et al. 2020 for air pollution in Iran, and Maranzano et al. 2023; Fassò et al. 2022; Calculli et al. 2015 for Italy). Notably, there are further applications in other fields, such as modelling bike-sharing

data or coastal profiles (see Piter et al., 2022; Otto et al., 2021). HDGM is a linear mixed effects model with a specific structure of the random effects capturing the spatiotemporal dynamics of environmental data, which are widely applied in diverse areas (see, e.g., Jiang and Nguyen 2007 for an overview). Second, GAMM has been employed in various areas, such as ecology (Knappe, 2016; Kneib et al., 2011), psychology (Bono et al., 2021), economics (Fahrmeir and Lang, 2001), psycholinguistics (Baayen et al., 2017), or event studies (Maranzano and Pelagatti, 2023). Third, needless to say, models based on decision trees have demonstrated their effectiveness in capturing complex patterns in different fields (see, e.g., Belgiu and Drăguț 2016 for an overview in remote sensing, or Qi 2012 for bioinformatics), particularly in combination with kriging approaches, e.g., in environmental (Sekulić et al., 2020; Chen et al., 2019; Guo et al., 2015), or air pollution studies (Liu et al., 2018, 2019). We refer the interested reader to the systematic literature review of (Patelli et al., 2023) for a structured overview of these approaches. Furthermore, an interesting new approach is to use deep neural networks for the prediction and interpolation of spatial data (see Nag et al., 2023; Daw and Wikle, 2023). Hybrid models, integrating different models in one single framework and exhibiting good robustness and adaptability, can combine the advantages of different models during the different stages of the modelling phase. Their adoption is rapidly increasing in various fields and predictions, including $PM_{2.5}$ (e.g., Bai et al., 2022; Tsokov et al., 2022; Sun and Xu, 2022; Wang et al., 2019; Ding et al., 2021), greenhouse gas emissions (Javanmard and Ghaderi, 2022), tea yield (Jui et al., 2022), depopulation in rural areas (Jato-Espino and Mayor-Vitoria, 2023), or disease monitoring (Kishi et al., 2023) and calibration of citizen-science air quality data (Bonas and Castruccio, 2021).

All three models account for the intrinsic spatial, temporal, and spatiotemporal dynamics of the $PM_{2.5}$ concentrations. This temporal and spatial dependence arises from the persistence of the particles in the atmosphere over a certain time and, simultaneously, from the displacement and spread of the particles to nearby areas, e.g., by wind (Merk and Otto, 2020). Previous studies successfully employed several statistical models to model air pollution scenarios in Northern Italy, such as generalised additive models (Bertaccini et al., 2012), Bayesian hierarchical models based on the stochastic partial differential equation approach (Cameletti et al., 2013; Fioravanti et al., 2021), or random forests (Stafoggia et al., 2019). In a comparative study for Northern Italy, Cameletti et al. (2011) studied the effectiveness of different statistical models in a Bayesian framework. Machine learning algorithms, including random forests, are

adept at capturing nonlinearities and interactions. Still, when applied to air quality modelling, the spatiotemporal nature of the phenomenon is often ignored (see, e.g., Fox et al., 2020). Consequently, the model’s performance deteriorates, with worse outcomes than those obtained from Kriging with External Drift (KED), considered standard for modelling spatiotemporal phenomena. KED shows better results than random forest in Lombardy (Fusta Moro et al., 2022) and in the USA (Berrocal et al., 2020). On the other hand, machine learning algorithms outperform classical models if spatiotemporal dependence is not considered at all (Kulkarni et al., 2022). Lu et al. (2023) compared geostatistical and ML models for NO₂ concentrations in Germany. Despite the limited number of studies comparing geostatistical and ML models, this subject is gaining increasing interest because the comparison provides valuable insights into the dynamics of the process, as we will illustrate below.

The remaining sections of this paper are organised as follows. Section 2 describes the general framework of the study and the data set used for our comparisons. Then, we explain the theoretical background of all considered models in Section 3. The comparative study is presented in Section 4, including fitting procedure (Section 4.1), residual analysis (Section 4.2), prediction performances within the cross-validation scheme (Section 4.3), and model interpretation (Section 4.4). Section 5 concludes the paper.

2 Data

Our comparative analysis is based on the *Agrimonia data set*, a comprehensive daily spatiotemporal data set for air quality modelling available open-access on Zenodo (Fassò et al., 2023). Specifically, it includes air pollutant concentrations and important covariates for all 141 stations of the air quality monitoring network in the Lombardy region and a 30 km buffer zone around the administrative boundaries. The data originates from multiple sources with different temporal and spatial resolutions. Using suitable aggregation and interpolation techniques described in Fassò et al. (2023), the *Agrimonia data set* is available on a daily basis for all ground-level measurement stations in the study area. It spans six years, from 2016 to 2021, and includes daily air pollutant concentrations, weather conditions, emissions flows, land use characteristics, and livestock densities. We summarise all variables considered in this study in Table 1, including their main descriptive statistics.

The response variable is the $\text{PM}_{2.5}$ concentration at the ground described in ensuing Section 2.1 in more detail, while the selected remaining variables of the *Agrimonia data set* serve as explanatory variables or features. They are summarised and motivated in Section 2.2.

2.1 $\text{PM}_{2.5}$ concentrations

The *Agrimonia data set* includes daily observations of several atmospheric pollutants retrieved from the Italian air quality monitoring network. Not all monitoring stations are equipped with the same sensors, so we have excluded locations where stations were not measuring $\text{PM}_{2.5}$, which is the target pollutant of this study. The 49 remaining stations are depicted in Fig. 1 (left) along with information about the type of surrounding area (rural, suburban, urban) and the primary nearest emission source (background, industrial, traffic), according to the EU classification (European Environmental Agency, 2022b). To depict the spatial variation of the PM concentrations, we coloured the stations according to the average daily concentration across the entire time period on the right-hand map in Fig. 1.

We consider the period from 2016 to 2020. The temporal variation of the observed $\text{PM}_{2.5}$ concentrations, grouped by months and by type of area, is displayed through a series of box-plots in Fig. 2. The colours are chosen according to the type of the surrounding area. Not surprisingly, there is a clear seasonality with higher concentrations in winter due to meteorological conditions resulting in reduced air circulation. The median concentrations range between $10\mu\text{gm}^{-3}$ and $40\mu\text{gm}^{-3}$ across the year. Thus, throughout the year, the median concentration was beyond the threshold of $5\mu\text{gm}^{-3}$ considered hazardous by the World Health Organisation guidelines (WHO, 2021). From Fig. 2, it is clear that all different types of areas are similarly affected by poor air quality. This spatial homogeneity is also visually confirmed in the map of Fig. 1 where clusters of similar neighbouring concentrations can be seen, suggesting a pronounced spatial dependence.

To explore a possible spatiotemporal correlation, we estimate a spatiotemporal variogram $\gamma(h, \tau)$ based on the sample variance of observations within certain distance ranges in space and time h and τ (see, e.g., Cressie and Wikle, 2015). Smaller values of the variogram for smaller distances indicate (short-term) statistical dependence. The spatiotemporal variogram of observed $\text{PM}_{2.5}$ concentrations is depicted in Fig. 3. As expected, the variogram identifies an apparent correlation of the $\text{PM}_{2.5}$ concentrations across time and space. More precisely, the

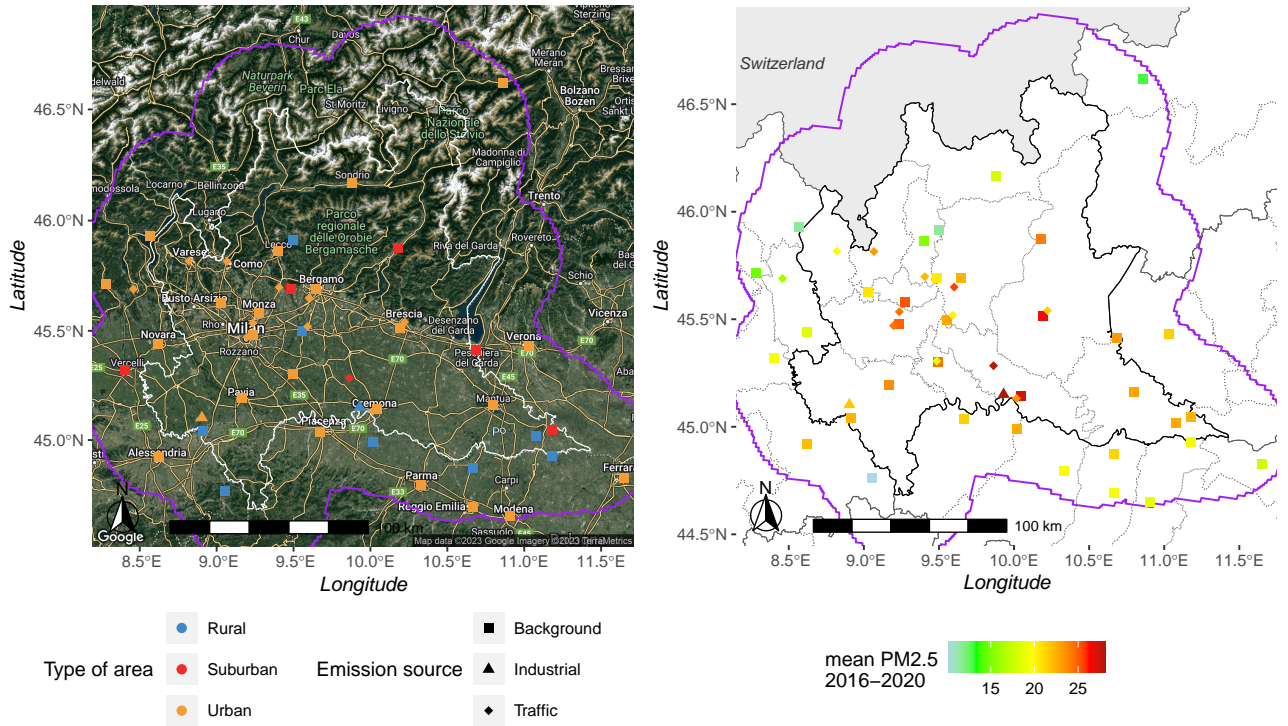


Figure 1: Map of the 49 PM_{2.5} monitoring stations extracted from the *Agrimonia data set*. The purple line represents a 0.3° buffer around the administrative boundaries of the Lombardy region, the latter represented by the white line. Left: Stations are coloured according to the type of area. The shape indicates the main emission sources. Right: the stations are coloured according to the 2016-2020 average PM_{2.5} concentrations [$\mu\text{g m}^{-3}$] over 2016-2020.

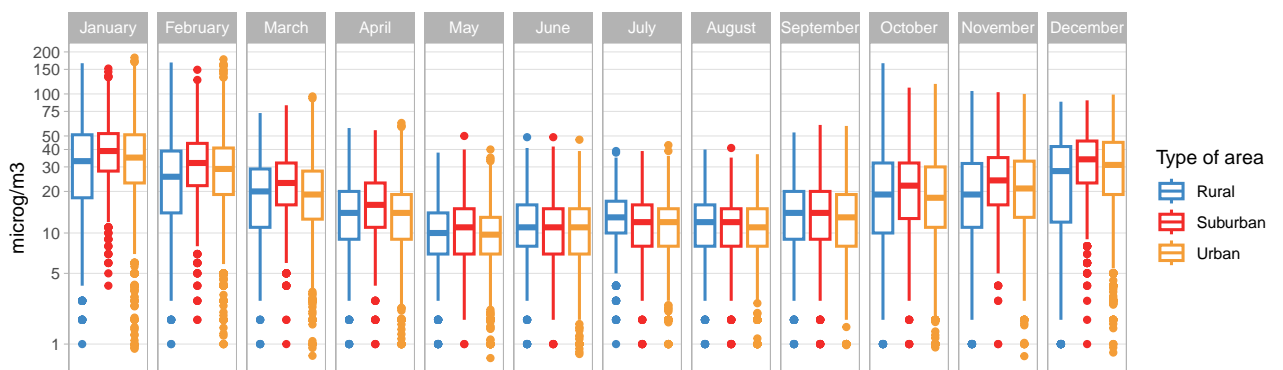


Figure 2: Monthly boxplots of PM_{2.5} concentrations (on a log scale) measured in Lombardy, including the buffer area.

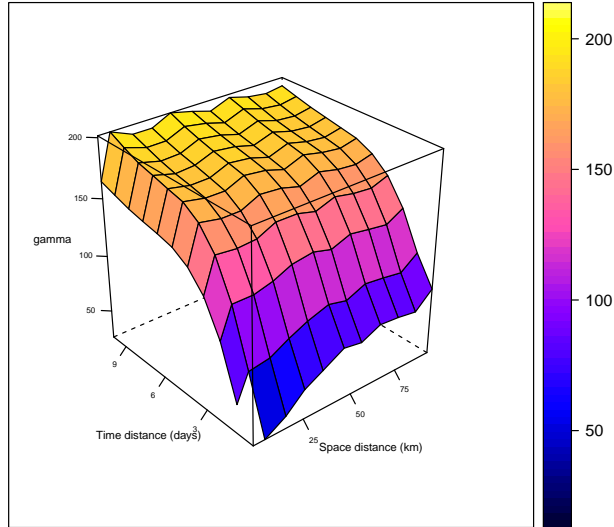


Figure 3: Spatiotemporal variogram of the $PM_{2.5}$ concentrations.

values of the variogram for the first temporal lags indicate a pronounced temporal dependence within the first 5-6 days, i.e., approximately one week. Furthermore, we observe a noticeable spatial dependence since the variogram increases with increasing spatial distances. It is important to note that this variation still includes spatial and temporal seasonalities and variations caused by exogenous factors.

2.2 Regressors

All models, which will later be used for the comparison, share the same set of regressors, including weather conditions and livestock densities. Based on an extensive literature review on air pollution modelling, we carefully selected key weather variables and incorporated information regarding local-scale animal breeding. The specific variables considered are presented in Table 1 and their corresponding descriptive statistics. Furthermore, monthly indicator variables are included to capture the seasonality, as highlighted by Fig. 2. Below, we will provide a brief motivation for each variable and the descriptive statistics in Table 1 to offer an intuitive understanding of the explanatory variables.

Firstly, several studies have found that weather is a crucial factor in air quality modelling (Bertaccini et al., 2012; Ignaccolo et al., 2014; Merk and Otto, 2020; Fassò et al., 2022; Grange

Table 1: Variables selected from the *Agrimonia data set*. Names are consistent with the data set (Fassò et al., 2023) and the accompanying data descriptor (Fassò et al., 2023).

Variable - Description [unit of measure]	Min	Mean	St. Dev.	Max
Altitude Height in relation to sea level [<i>m</i>]	4	171.458	200.004	1,194
AQ_pm25 Fine particulate matter concentrations [μgm^{-3}]	0.506	20.896	16.353	182
WE_temp_2m Air temperature at 2 m [$^{\circ}\text{C}$]	-20.650	12.916	8.233	32.880
WE_tot_precipitation Total precipitation [<i>m</i>]	0	0.003	0.008	0.172
WE_rh_mean Relative humidity [%]	19.490	74.433	12.299	99.520
WE_wind_speed_100m_mean Average wind speed at 100m [<i>m/s</i>]	0.564	2.550	1.326	11.930
WE_blh_layer_max Daily maximum height of the air mixing layer layer [<i>m</i>]	13.790	1,039.402	556.877	4,421.000
LI_pigs_v2 Average density of pigs bred for the area (10km ²) surrounding the measurement stations [<i>number/km</i> ²]	0.022	115.215	159.666	652.100
LI_bovine_v2 Average density of bovine bred for the area (10km ²) surrounding the measurement stations [<i>number/km</i> ²]	1.543	46.241	47.463	178.800
LA_hvi High vegetation abundance [<i>m</i> ² / <i>m</i> ²]	0.861	2.324	0.804	5.034
LA_lvi Low vegetation abundance [<i>m</i> ² / <i>m</i> ²]	0.865	2.208	0.560	3.662

et al., 2023; Chang and Zou, 2022). Changes in weather conditions such as temperature, precipitation, and wind speed and direction can affect atmospheric stability and turbulence, which can influence the transport and deposition of pollutants. For instance, temperature and boundary layer height are usually negatively related to air pollutant concentrations. Similarly, we typically observe reduced PM concentrations during periods with increased precipitation or wind speed. On the contrary, the direction and size of the effect of the relative humidity are still debated, but it undoubtedly affects the PM_{2.5} concentrations (Zhang et al., 2017).

Secondly, we considered agricultural influences, which appear to impact air quality (e.g., Thunis et al., 2021; Lovarelli et al., 2020). The Livestock (LI) data used in this study provide information on the average density of pigs and cattle per municipality (expressed as animals per km²) in the vicinity of each station (within a radius of 10km²). Including livestock data is essential to capture the impact of ammonia (NH₃) emissions on air quality, as livestock farming is the major source of NH₃ emissions (up to 95%). Therefore, including LI data in air quality modelling can help better understand and mitigate livestock’s impact on air pollution levels.

3 Spatiotemporal statistical models and machine learning techniques

We consider the PM_{2.5} concentrations as realisations of a spatiotemporal stochastic process $\{Z(s, t) : s \in D, t = 1, 2, \dots, T\}$, where D is the spatial domain that contains a set of locations $\{s_i : i = 1, \dots, n\}$ (i.e., the ground-level measurement stations) and the temporal domain is discrete $t = 1, \dots, T$ (i.e., daily observations). Furthermore, we posit that $Z(s, t)$ might be influenced by external variables related to weather conditions, emissions, or agricultural activities. Throughout the remainder of the paper, the terms regressors, covariates, and features are used interchangeably. The spatiotemporal proximity of observations typically induces statistical dependence, and thus, the selected model candidates should appropriately incorporate this inherent spatiotemporal dependence. To structure the model alternatives, we can decompose the models into three terms, i.e.,

$$Z(s, t) = S(s, t) + U(s, t) + \varepsilon(s, t), \quad (1)$$

where $S(s, t)$ is the large-scale component including the regressors, $U(s, t)$ includes small-scale spatiotemporal effects, and $\varepsilon(s, t)$ comprises the measurement and modelling errors, which are

assumed to be a zero-mean white noise process.

3.1 Hidden dynamic geostatistical model

The first model selected is the HDGM, which serves as the comparative analysis' starting point or baseline method. It is a widely applied geostatistical model, first considered by Huang and Cressie (1996) as an extension of classical mixed-effects models for univariate spatiotemporal data. Calulli et al. (2015) extended the HDGM to multivariate data. This modelling approach proved particularly useful for air quality modelling (e.g., Fassò and Finazzi, 2011; Finazzi et al., 2013), as the comparative study of Cameletti et al. (2011) confirmed. The HDGM specifies the large-scale effects as a linear regression model, i.e.,

$$S(s, t) = \mathbf{X}_\beta(s, t)' \boldsymbol{\beta}, \quad (2)$$

where $\boldsymbol{\beta} = (\beta_0, \dots, \beta_p)'$ is a vector of p fixed-effect coefficients, including the model intercept β_0 , and $\mathbf{X}_\beta(s, t)$ is the (s, t) -th entry of the fixed design matrix of the selected covariates/features. In other words, $\mathbf{X}_\beta(s, t)$ is the vector of the observed covariates at location s and time point t .

The spatiotemporal dependence is modelled as small-scale effects by a geostatistical process

$$U(s, t) = v\xi(s, t), \quad (3)$$

where v is an unknown, homoscedastic scaling factor, which has to be estimated and describes the degree of the small-scale effects. Further, $\xi(s, t)$ is a latent random variable with Markovian temporal dynamics given by

$$\xi(s, t) = g_{HDGM}\xi(s, t - 1) + \eta(s, t), \quad \eta(s, t) \sim GP, \quad (4)$$

where $g_{HDGM}\xi(s, t - 1)$ is a hidden first-order autoregressive process with coefficient g_{HDGM} . The temporal dependence is separated from the spatial interactions, which are modelled in $\eta(s, t)$. It is worth noting that this implies a separable space-time covariance. Specifically, $\eta(s, t)$ is a Gaussian process (GP) with zero mean, unit variance, and covariance matrix determined by an exponential spatial correlation function

$$\rho(\|s - s'\|; \theta_{HDGM}) = \exp(-\|s - s'\|/\theta_{HDGM}) \quad (5)$$

with θ_{HDGM} being the range parameter, s and s' are two distinct spatial locations, and the distance between them is given by the vector norm $\|\cdot\|$. For this study, we will always employ

the distance on the great circle, i.e., the length of the geodesic between s and s' . The parameters of the random effects process $\xi(s, t)$ are assumed to be in a space leading to a weakly stationary spatiotemporal process. Finally, $\varepsilon(s, t)$ is an identically distributed random error independent across space and time with zero mean and a constant variance σ_ε^2 .

The model parameter set $\Phi = \{\beta, g_{HDGM}, \theta_{HDGM}, \nu, \sigma_\varepsilon^2\}$ is estimated by the maximum-likelihood method using an expectation-maximisation (EM) algorithm (Calculli et al., 2015). The estimation procedure is computationally implemented in the MATLAB software package D-STEM (see Wang et al., 2021).

3.2 Generalised additive mixed model

Compared to generalised additive models (GAM, Hastie and Tibshirani 1987), generalised additive mixed models (GAMM) include a random-effects component to describe correlated response variables, such as time series, spatial or spatiotemporal data. It extends the HDGM by allowing for linear and nonlinear regressive effects in a GAM fashion, i.e., the response variable linearly depends on smooth functions of the predictors. To be precise, the large-scale components are given by

$$S(s, t) = \mathbf{X}_{linear}(s, t)' \boldsymbol{\beta}_{linear} + \underbrace{\sum_{j=1}^m \alpha_{(j)}(\mathbf{X}_{nonlinear, j}(s, t))}_{\text{nonlinear effects}} \quad (6)$$

with $\mathbf{X}_{linear}(s, t) \boldsymbol{\beta}_{linear}$ being a linear parametric regression term of the first k covariates with a parameter vector $\boldsymbol{\beta}_{linear} = (\beta_0, \beta_1, \dots, \beta_k)'$, including the intercept term β_0 . Moreover, $\sum_{j=1}^m \alpha_{(j)}(\mathbf{X}_{nonlinear, j}(s, t))$ is an additive term with nonlinear influence functions $\alpha_{(j)} : \mathbb{R} \rightarrow \mathbb{R}$ of the j -th column in $\mathbf{X}_{nonlinear, j}$ for the remaining m regressors. These nonlinear influences can be estimated along with the other model coefficients, e.g., as regression splines or penalised splines (Fahrmeir et al., 2004).

The small-scale effects of the GAMM are specified as a first-order autoregressive model for the temporal dependence and a smooth spatial surface for the spatial dependence, that is,

$$U(s, t) = g_{GAMM}(Z(s, t - 1) - S(s, t - 1) - C(s)), \quad (7)$$

where g_{GAMM} is the parameter representing the temporal dependence, where zero indicates no temporal correlation. The spatial dependence is modelled as a smooth surface $C(s)$, which

follows a Gaussian process with an exponential covariance function with the range parameter θ_{GAMM} (Handcock and Wallis, 1994). This structure is identical to the spatial term of the random effects model in HDGM as given by equation (5). In our case, θ_{GAMM} is estimated as proposed by Kammann and Wand (2003). The model estimation is computationally implemented in the package `mgcv` available in R (Wood, 2017).

3.3 Random forest spatiotemporal kriging

For the third approach, RFSTK, we increase the flexibility of the model in the large-scale component by considering a random forest (RF) algorithm. In other words, the third hybrid model combines an RF for the large-scale component $S(s, t)$ with that of a spatiotemporal kriging model for $U(s, t)$. The idea traces back to the combination of random forests and kriging, the so-called random forest residual kriging, which – even if only considering spatial dependence – showed promising results compared to RF alone (e.g. Wang et al., 2019; Viscarra Rossel et al., 2014). For spatiotemporal data, RFSTK has been considered to model air quality – again showing good performances (see Zhan et al., 2018; Shao et al., 2020).

Random forests are widely used tools in machine learning as an ensemble of multiple decision trees (Breiman, 2001). In a regression problem, the prediction of the large-scale effect is obtained by averaging across the predictions of n_{tree} decision trees, which are trained/estimated from independent bootstrap samples Z_j^* of the input data ($j = 1, \dots, n_{\text{tree}}$), i.e.,

$$S(s_i, t) = \frac{1}{n_{\text{tree}}} \sum_{j=1}^{n_{\text{tree}}} \widehat{E}(Z_j^*(s_i, t) \mid \mathbf{X}(s_i, t) : i = 1, \dots, n, t = 1, \dots, T), \quad (8)$$

where $\widehat{E}(Z_j^*(s_i, t) \mid \cdot)$ is the prediction of the j -th decision tree. For regression trees, it is important to notice that the averaging should be done for each region of interest in the covariate space.

The small-scale model of RFSTK is assumed to be a zero-mean, weakly stationary spatiotemporal Gaussian process

$$U(s, t) = \tilde{\eta}(s, t) \sim GP, \quad (9)$$

where the covariance matrix is obtained from a separable space-time correlation function given by

$$\rho(\|s - s'\|, |t - t'|) = \rho(\|s - s'\|; \theta_{RFSTK_s}) \cdot \rho(|t - t'|; \theta_{RFSTK_t}) \quad (10)$$

with $\|s - s'\|$ and $|t - t'|$ representing spatial and temporal distances between (s, t) and (s', t') , respectively. That is, the exponential correlation functions are equivalent to the spatial correlation function of the HDGM and GAMM, but the other two approaches consider an autoregressive temporal dependence, while the RFSTK employs a continuous correlation function for both the temporal and spatial dependence. The parameters and decision trees are estimated in a two-step procedure. First, predictions for the large-scale component are obtained using RFs, computationally implemented in the R package `randomForest` (Liaw and Wiener, 2002). Second, to adjust the predictions of the RF accounting for space-time interactions, the parameters of the separable space-time correlation function in (10) are estimated by variography on RF residuals, implemented in the R package `gstat` (Gräler et al., 2016).

4 Comparative study

In the subsequent section, we present an application of each methodology on air quality data extracted from the *Agrimonia data set* (see Section 2). We start with exploring the model fitting process and examining the residuals. Subsequently, we evaluate the predictive performances of the models through cross-validation. Finally, our attention shifts to the interpretation of each model and its comparison. Drawing upon this comparison, we offer practical suggestions for integrating the modelling outcomes into other environmental analyses.

4.1 Model fitting

For the HDGM, we express the large-scale component $S(s, t)$ in the Wilkinson notation (Wilkinson and Rogers, 1973) as follows (see Table 1 for variable acronyms):

$$\begin{aligned}
 \text{AQ_pm25} \sim & 1 \\
 & + \text{Altitude} + \text{Month} \\
 & + \text{WE_wind_speed_100m_mean} + \text{WE_temp_2m} \\
 & + \text{WE_tot_precipitation} + \text{WE_rh_mean} + \text{WE_blh_layer_max} \\
 & + \text{LA_lvi} + \text{LA_hvi} \\
 & + \text{LI_pigs_v2} + \text{LI_bovine_v2} .
 \end{aligned} \tag{11}$$

To ensure the comparability of the results across all three model alternatives, we considered all predictors in their original scale. Transformations such as a logarithmic transformation of the response variable did not generally yield better prediction results and model fits. This suggests an additive structure in the large-scale effects, and its coefficients can directly be interpreted as marginal (linear) effects.

The large-scale component $S(s, t)$ of GAMM captures nonlinear effects by estimating a functional relationship between the predictors and the response variable. Identifying predictors requiring nonlinear relationships entailed simulating model residuals from a linear regression model and graphing them alongside their corresponding predictors, including confidence intervals, as suggested in Fasiolo et al. (2020). A smooth nonlinear effect is estimated if a pattern outside the confidence bands is detected. In this study, all continuous variables, except for altitude, required a smooth term represented by a cubic regression spline. The large-scale component $S(s, t)$ of GAMM in (6) is given by

$$\begin{aligned}
 \text{AQ_pm25} &\sim 1 \\
 &+ \text{Altitude} + \text{Month} \\
 &+ s(\text{WE_wind_speed_100m_mean}) + s(\text{WE_temp_2m}) \\
 &+ s(\text{WE_tot_precipitation}) + s(\text{WE_rh_mean}) + s(\text{WE_blh_layer_max}) \\
 &+ s(\text{LA_lvi}) + s(\text{LA_hvi}) \\
 &+ s(\text{LI_pigs_v2}) + s(\text{LI_bovine_v2}),
 \end{aligned} \tag{12}$$

where $s(\cdot)$ denotes a smooth potentially nonlinear function, $\alpha_{(j)}(\cdot)$ in (6). For our analysis, we have chosen cubic splines. The spatial dependence is modelled within the GAMM as a two-dimensional smooth surface $C(s)$ governed by a zero-mean Gaussian process with an exponential covariance function, while the temporal dependence is represented by an autoregressive term of order one. The model is estimated through the restricted maximum likelihood method using the package `mgcv` in R (Wood, 2011).

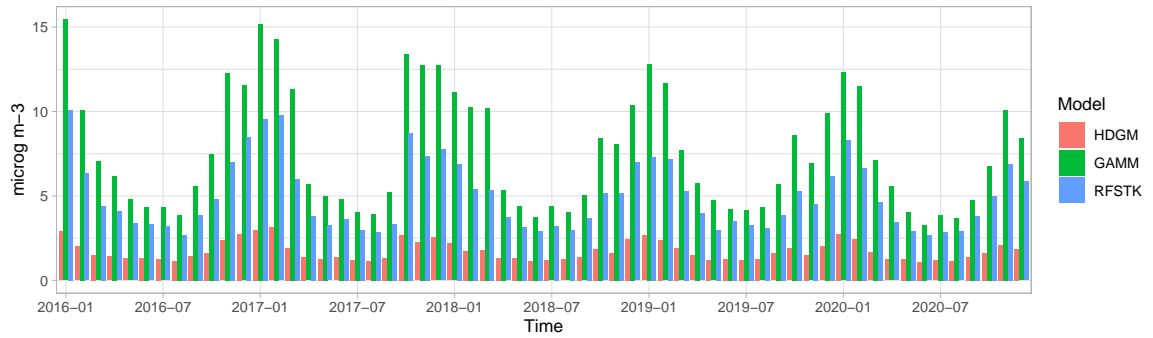
To optimise the performance of RF, we evaluate the trade-off between prediction accuracy and computation time across various hyperparameter settings. The latter include the number of trees n_{tree} , the number of candidate predictors for building each tree, and the size of the final leaves of each tree. Our findings indicate that utilising default settings (500 trees, the number of candidate variables equal to one-third of the number of the predictors, and final leaf size of 5) within the R package `randomForest` (Liaw and Wiener, 2002) is suitable. Then,

Table 2: In-sample performance of the three models assessed by RMSE (in μgm^{-3}), and the adjusted coefficient of determination R^2 . The fit of the only large-scale component (LS) is compared to the full model (FM).

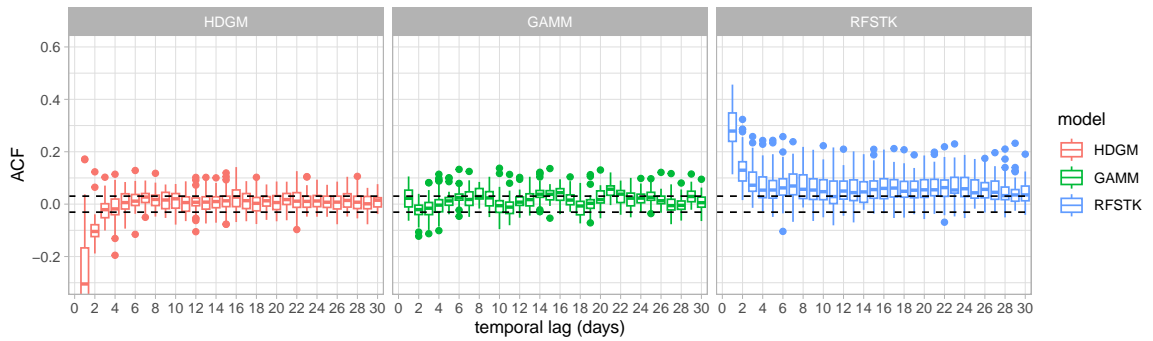
	HDGM		GAMM		RFSTK	
	LS	FM	LS	FM	LS	FM
RMSE [μgm^{-3}]	11.92	1.814	11.456	8.468	8.245	5.361
R^2	0.469	0.988	0.509	0.732	0.746	0.893

RF predictions are adjusted by adding RF residual predictions obtained by fitting an ordinary spatiotemporal kriging model by using the R package `gstat` (Gräler et al., 2016).

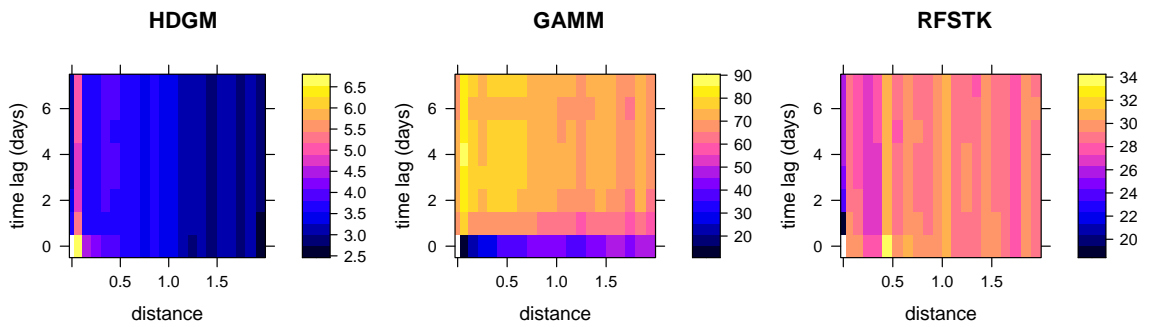
To highlight the difference between the model fits, we compared the in-sample (i.e. using the entire data set) predictive performance of all the models, separately for the large-scale component (LS) and the full model (FM), including the space-time effects. It is worth noting that we included $C(s)$ in the constant term of the LS component for GAMM, allowing for direct comparisons with the HDGM fit of the regression terms. The comparison was based on the root mean squared errors (RMSE), mean absolute errors (MAE), and the coefficient of determination R^2 . The results are reported in Table 2. HDGM generally had better prediction capabilities and lower computational costs than the other models when we consider the full model. The RFSTK model had relatively good prediction capabilities but was computationally intensive, particularly when including the spatiotemporal kriging. For our dataset, the GAMM model had the lowest in-sample fit. However, the informativeness of the in-sample results can be questionable due to the potential sensitivity of models to the training data or overfitting. To address this issue, we evaluated prediction performances within a cross-validation scheme, which is explained in Section 4.3. For instance, this analysis revealed that the HDGM could generalise the estimated relation to obtaining outperforming out-of-sample predictions across space, while we observe a serious overfit in the in-sample case due to the flexibility of the random-effects model. We will focus on this result in more detail below.



(a) Standard deviation of residuals grouped by months and models.



(b) Boxplots (across stations) of residuals' temporal correlograms for the three models.



(c) Sample spatiotemporal variogram of the residuals of each model. Spatial distances are expressed in Earth degrees.

Figure 4: In-sample residual diagnostics for the three models.

4.2 Residual analysis

The residual distributions are symmetric and slightly leptokurtic, which means there is a greater chance of extreme values than a normal distribution, indicating that all models are less reliable at predicting extreme events. This is not surprising as they are designed to predict the mean level of the distribution and not for modelling the extremes.

The model uncertainties across time, shown in Figure 4a, where the standard deviation of the residuals is depicted for each month, reveal that all three models have varying uncertainty throughout the year. More precisely, the PM concentrations in the winter periods could be less accurately predicted than in the summer periods. Therefore, when the models are implemented for forecasting or scenario analysis, it is recommended to use a heteroscedastic model to not underestimate the prediction accuracy in the winter months (or overestimate for the summer period). For instance, spatiotemporal stochastic volatility models could be estimated for the residual process, as demonstrated in Otto et al. (2022) for much simpler mean models. However, in this paper, our focus will be on the comparison of the mean predictions of the three models.

Furthermore, we investigated the spatial and temporal dependence of the residuals estimating temporal autocorrelation functions (ACF) and spatiotemporal variograms. The results are shown in Figures 4b and 4c. Different patterns were observed across the three models. While HDGM shows a small negative correlation at the beginning, indicating a slight overestimation of the temporal dependence, the spatial correlation is satisfactorily captured. On the contrary, GAMM leads to significantly lower temporal correlations in the residuals but does not capture the spatial dependence, as highlighted by the variogram through the bottom line for time lag 0. The RFSTK is characterised by a more pronounced positive autocorrelation for the first 3-4 lags, as shown by the correlogram (ACF), consistently with the model specification that does not consider an autoregressive term. The spatiotemporal correlation was clearly captured, as confirmed by the flat variogram. It is worth noting that the scales of the variograms differ significantly. This is because the prediction performances of the models also differ significantly in the in-sample case.

4.3 Cross-validation and comparison of predictive performance

We employed the leave-one-station-out cross-validation (LOSOCV) scheme, which is a variation of the commonly used leave-one-out cross-validation approach applied in the spatiotemporal

framework (e.g., Meyer et al., 2018; Nowak and Welsh, 2020). For this method, a complete time series of a single station withheld is not used in the model’s training but is used to evaluate the model’s prediction performance. In this way, the validation blocks are sufficiently large not to destroy the spatiotemporal dependence. All stations within the Lombardy region were used for validation, except for the station “Moggio.” It is located in the mountains with unique climatic conditions that are not well-represented by all other stations. After implementing the LOSOCV approach, we obtained prediction results for the 31 stations included in the validation process. It is worth noting that we applied the identical cross-validation scheme for each model so that the results are directly comparable.

The prediction performances assessed in the LOSOCV scheme in terms of mean squared errors (MSE), RMSE, MAE, and R^2 are summarised in Table 3. HDGM is confirmed to be the best model, but – compared to the in-sample residuals in Table 2 – the uncertainty is on a realistic level with an RMSE comparable to the other models. That is, the overfit in the in-sample data did not affect the generalisation ability of the HDGM. This could be due to the linear structure in the large-scale component. While a more flexible model (e.g., random forest or artificial neural networks) could produce extremely bad predictions in areas of insufficient training data or overfitting, the linear structure of the HDGM regression term prevents us from obtaining such extreme predictions. Generally, we observe satisfactory prediction performances for all three model alternatives, with GAMM and the RFSTK approach being in second and third place, respectively. The substantial difference between the in-sample residuals from the model trained on the entire dataset and the errors from the LOSOCV scheme highlights the importance of validating prediction uncertainty through a cross-validation scheme, which accounts for the spatiotemporal nature of the data. Interestingly, the GAMM obtained a similar fit in terms of the coefficient of determination in both the in-sample case and the cross-validation. Thus, we would not overestimate the prediction capabilities when only looking at the in-sample fit.

Eventually, we compare the prediction performances for each station separately because we observed that the order of the best-fitting model is not homogeneous across space. For this reason, Figure 5 displays the cross-validation RMSE on a map by the size of differently coloured circles. That is, the colour of the smallest circle at each station corresponds to the model with the best prediction performance, whereas the largest circles show the worst predictions. Below, we will discuss two selected cases with interesting behaviour: “Lecco - Via Sora” (station

Table 3: Prediction performance indices evaluated with the LOSOCV scheme [μgm^{-3}]

	MSE	RMSE	MAE	R^2
HDGM	35.373	5.948	4.376	0.879
GAMM	78.042	8.834	6.239	0.733
RFSTK	53.099	7.286	5.119	0.819

706) and “Como - Via Cattaneo” (station 561). Furthermore, we depict the cross-validation prediction errors across time for these two stations in Fig. 6.

HDGM and RFSTK performed worse than GAMM at the station “Lecco - Via Sora” (station ID 706). This is because Lecco is characterised by good air quality, but its neighbouring areas are affected by high $\text{PM}_{2.5}$ concentrations. The GAMM model, which does not include strong, time-varying spatial interactions, was able to capture this difference in air quality better than the HDGM and RFSTK models. This is confirmed by the fact that the 15-day moving average of the test errors (calculated as observed minus predicted) displayed in Fig. 6 shows that both HDGM and RFSTK overestimate the $\text{PM}_{2.5}$ concentrations at this station.

At the other selected station, “Como - Via Cattaneo” (station ID 561), the RFSTK model performed the worst while HDGM showed the best performance. The reason may lie in its poor ability to capture temporal dependence well. The concentrations of $\text{PM}_{2.5}$ at this station are very stable over time, and the RFSTK model does not fully capture this stability. This is shown by the 15-day moving average of the test errors in Fig. 6, which shows that RFSTK underestimates $\text{PM}_{2.5}$ concentrations, especially in the winter periods, when the air circulation is at its lower limit and temporal stability is the highest.

These results highlight the need to select the model according to the local conditions carefully. The best model for one location may not be the best for another. Moreover, model averaging could additionally improve the predictions.

4.4 Model interpretation

In the following three sections, we delve into the outcomes derived from our models, offering a comprehensive interpretation of each estimated model.

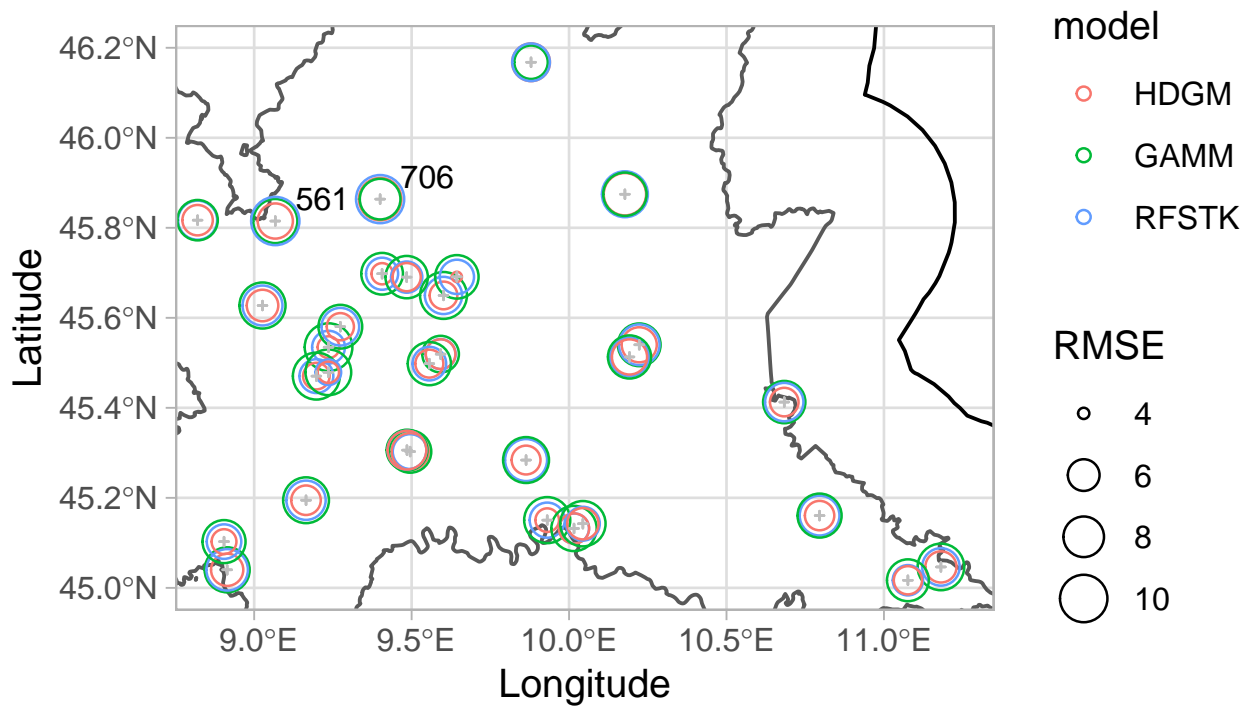


Figure 5: Prediction performances expressed as RMSE calculated for each station within the LOSOCV scheme. The stations “Lecco - Via Sora” (ID 706) and “Como - Via Cattaneo” (ID 561) are labelled.

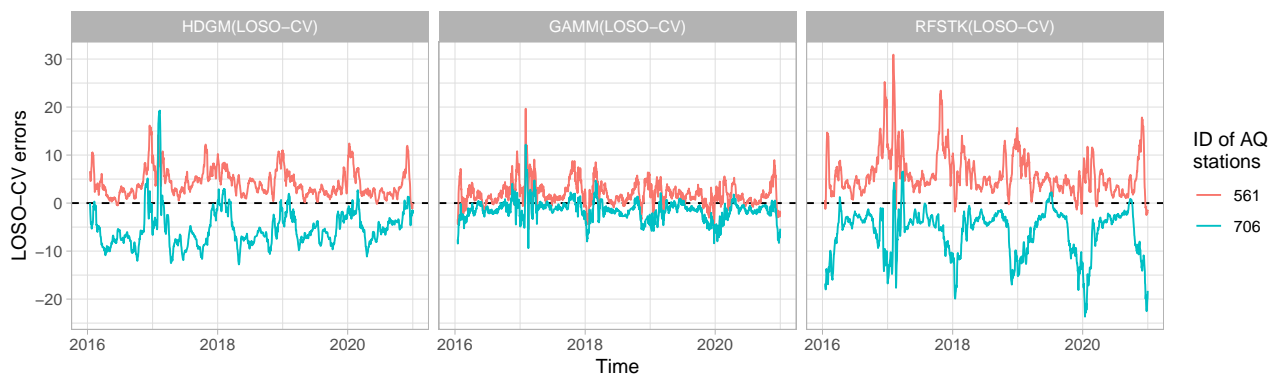


Figure 6: 15 days moving averages on the prediction errors (in $\mu\text{g}/\text{m}^3$) for each model (HDGM, GAMM and RFSTK from left to right)

Table 4: Estimated coefficients of the large-scale component of the HDGM model.

Variable	Coefficient	Std. Err.	t-value	p-value
(Intercept)	39.626	1.399	28.332	< 0.0001
February	-7.222	1.316	5.490	< 0.0001
March	-15.298	1.474	10.378	< 0.0001
April	-21.569	1.552	13.898	< 0.0001
May	-27.608	1.596	17.295	< 0.0001
June	-27.662	1.666	16.602	< 0.0001
July	-27.493	1.690	16.270	< 0.0001
August	-29.316	1.681	17.436	< 0.0001
September	-27.611	1.628	16.956	< 0.0001
October	-20.335	1.555	13.080	< 0.0001
November	-16.602	1.493	11.117	< 0.0001
December	-8.526	1.349	6.318	< 0.0001
Altitude	-0.007	0	20.180	< 0.0001
WE_wind_speed_100m_mean	-1.946	0.048	40.520	< 0.0001
WE_tot_precipitation	-159.416	7.145	22.310	< 0.0001
WE_temp_2m	0.505	0.037	13.595	< 0.0001
WE_rh_mean	0.186	0.008	24.188	< 0.0001
WE_blh_layer_max	-0.003	0	19.628	< 0.0001
LI_pigs_v2	0.005	0.001	9.288	< 0.0001
LI_bovine_v2	0.003	0.002	1.147	0.251
LA_lvi	-4.441	0.225	19.698	< 0.0001
LA_hvi	-0.494	0.141	3.507	< 0.0001

4.4.1 HDGM

Table 4 summarises the estimated β parameters of the large-scale component of HDGM. Except for bovine density (LI.bovine_v2), all coefficients significantly differ from zero. The signs of the majority of the coefficients are consistent with our expectations: summer months are related to reductions of $\text{PM}_{2.5}$ concentrations (about $-27/29 \mu\text{gm}^{-3}$), every 1m/s of wind speed is related to a decrease of $2 \mu\text{gm}^{-3}$ of $\text{PM}_{2.5}$, and every 10mm of precipitation are related to an expected decrease of $1.6\mu\text{gm}^{-3}$ of $\text{PM}_{2.5}$. Moreover, each degree Celsius increase in temperature is related to an increase of $0.5 \mu\text{gm}^{-3}$ of $\text{PM}_{2.5}$, which seems counter-intuitive at first glance. However, the temperature effect should be interpreted together with the monthly fixed effects. The relative humidity is positively related to $\text{PM}_{2.5}$, so high humidity levels (100%) are associated with an increase of $18 \mu\text{gm}^3$ with respect to extremely dry air. The maximum height of the boundary layer is negatively associated with $\text{PM}_{2.5}$; every increase of 1000m is related to an expected decrease of $3 \mu\text{gm}^{-3}$ of $\text{PM}_{2.5}$.

Regarding the agricultural impact, we observe that the number of pigs in the territory is positively associated, and an increase of 1000 animals per km^2 corresponds to an expected increase of $5 \mu gm^{-3}$ of $PM_{2.5}$. Both vegetation indices are negatively related to $PM_{2.5}$, while low vegetation (e.g. bushes) has a stronger effect than higher vegetation (e.g. trees).

The small-scale effect of the HDGM is defined by a latent variable $\xi(s, t)$ in (4), which has an autoregressive structure of order one and a Gaussian process with exponential covariance function given by (5). The spatial range parameter θ_{HDGM} describes the decay of the exponential correlation function and is estimated to be equal to 0.79° . Thus, there is a large spatial correlation (i.e., > 0.37) for surrounding stations in an area of 80 kilometres. The estimate of the temporal autoregressive parameter is equal to $\hat{g}_{HDGM} = 0.72$. This indicates that the time series has low-frequency components with relatively gradual changes over time.

4.4.2 GAMM

The estimated coefficients of our second model, the GAMM, are presented in Table 5. In the first section of the table, the estimated coefficients for the linear part of the model (including the monthly fixed effects) are reported, while the second part summarises the effective degrees of freedom of the nonlinear effects as a measure of complexity/non-linearity. Compared to HDGM, the monthly fixed effects are slightly smaller, indicating that the seasonal variation is better captured by the weather variables, which enter the model nonlinearly. Complex nonlinear relationships with large degrees of freedom characterised the smooth terms of the cubic regression splines. All of them are significant except for the density of bovine. To illustrate the difference between the linear effects in the HDGM and the nonlinear effects in GAMM, we depict some selected regression splines in Figure 7 along with the estimated linear functions of the HDGM. These curves correspond to the marginal effect of variables neglecting the spatiotemporal correlation (i.e., without the influence of neighbouring sites). In general, we observe a similar tendency for both models. An exceptional notice would be the height of the boundary layer, which has a negative effect for up to 500 kilometres, and afterwards, the effect changes to be positive. By contrast, the effect is negative for the HDGM, which mimics the effect in the areas where most observations are located. The grey contour lines in Fig. 7 additionally illustrate the estimated kernel density of the couple ($PM_{2.5}$, WE_regressor). We note that the confidence intervals around the fitted curves are smaller in areas with higher

Table 5: Estimated coefficients of the large-scale component of the GAMM. Linear relationships (A) are identified by the β coefficients, while for nonlinear relationships (B), the complexity of the curve is described by the effective degrees of freedom (edf).

<i>A: Linear effects</i>	Coefficient	Std. Err.	t-value	p-value
(Intercept)	37.3052	0.4541	82.1536	< 0.0001
February	-7.2787	0.3559	-20.4496	< 0.0001
March	-11.6052	0.4169	-27.8335	< 0.0001
April	-14.6751	0.5173	-28.3679	< 0.0001
May	-20.5547	0.6097	-33.7147	< 0.0001
June	-22.0366	0.6978	-31.5800	< 0.0001
July	-23.2506	0.7287	-31.9076	< 0.0001
August	-24.5223	0.6813	-35.9908	< 0.0001
September	-22.7519	0.5743	-39.6143	< 0.0001
October	-18.9167	0.4687	-40.3605	< 0.0001
November	-15.8692	0.4005	-39.6225	< 0.0001
December	-11.4140	0.3541	-32.2379	< 0.0001
Altitude	-0.0023	0.0012	-1.9378	0.0526
<i>B: Nonlinear effects</i>	edf	Ref.df	F-value	p-value
WE_temp_2m	8.5851	8.5851	267.3673	< 0.0001
WE_tot_precipitation	7.2891	7.2891	210.3836	< 0.0001
WE_rh_mean	8.0060	8.0060	602.4805	< 0.0001
WE_wind_speed_100m_mean	6.5219	6.5219	214.0715	< 0.0001
WE_blh_layer_max	8.8552	8.8552	278.6934	< 0.0001
LI_pigs_v2	7.9422	7.9422	7.2958	< 0.0001
LI_bovine_v2	3.7865	3.7865	1.2020	0.2962
LA_hvi	8.4121	8.4121	23.1429	< 0.0001
LA_lvi	7.4114	7.4114	82.1857	< 0.0001
Longitude, Latitude	27.7758	32.0000	19.0023	< 0.0001

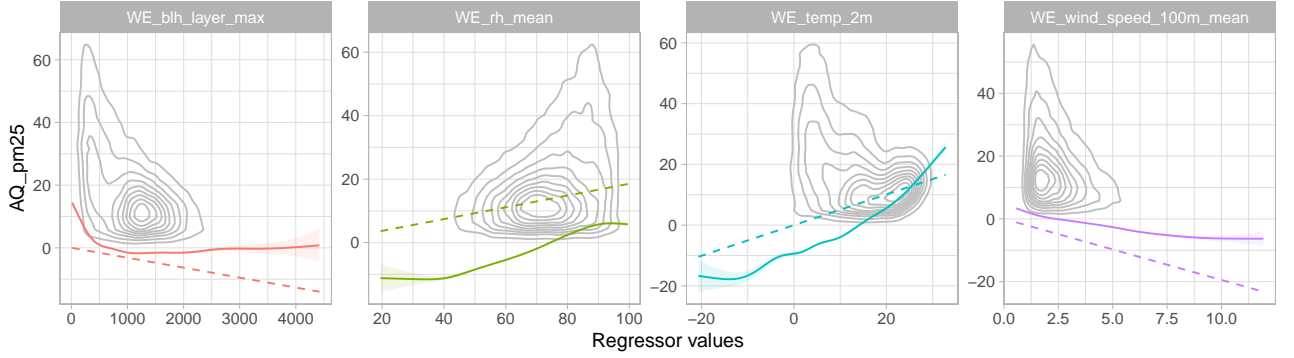


Figure 7: Smoothing splines (continuous lines), including their 95% confidence intervals (coloured shadows), and HDGM regression coefficients (dotted lines) for relevant weather regressors (i.e., boundary layer height, relative humidity, temperature, and wind speed). Grey contour lines represent the estimated two-dimensional kernel densities of the $\text{PM}_{2.5}$ concentrations and the corresponding regressors.

density.

The GAMM smooth spatial surface $C(s)$ is displayed in Fig. 8. This smoothing spline $C(s)$ capturing the spatial dependence identifies correlated areas. Our study shows higher concentrations of $\text{PM}_{2.5}$ in the area of Como and the area of Brescia, while in the southwest, corresponding to the Ligurian border, lower concentrations. Furthermore, the estimated range parameter of the exponential covariance function is $\hat{\theta}_{GAMM} = 1.16^\circ$, which corresponds to approximately 110 km. Hence, it is in a similar range to the other two models. Furthermore, the autoregressive parameter is estimated as $\hat{g}_{GAMM} = 0.67$, similar to HDGM and indicating a medium temporal persistence across one day. In this sense, the models show similar spatiotemporal dynamics as the HDGM.

4.4.3 RFSTK

The interpretability of the RFSTK model can be challenging due to its intricate nature. However, the variable importance factor (VIF) can help to identify the most important variables. To determine the VIF, the mean decrease accuracy technique is employed, which assesses the variables' importance by measuring the increase in MSE (IncMSE) when the values of the regressors are permuted (Breiman, 2001). The results are depicted in Fig. 9.

Like the previous models, the random forest cannot fully capture the seasonality by the

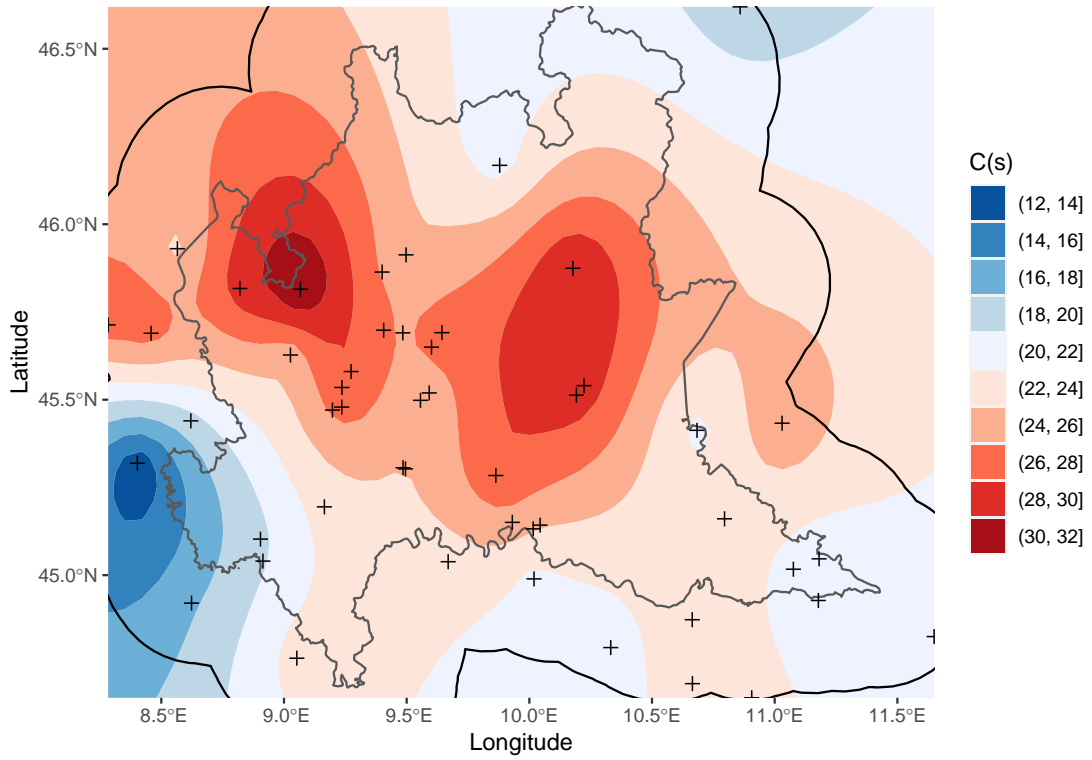


Figure 8: Estimated smoothing spline $\hat{C}(s)$ of GAMM, which corresponds to the $PM_{2.5}$ predicted on a regular grid using the large scale of GAMM, where all regressors are set to 0. Stations are marked with a black cross, Lombardy boundaries are shown in grey, and the black line marks the surrounding buffer zone.

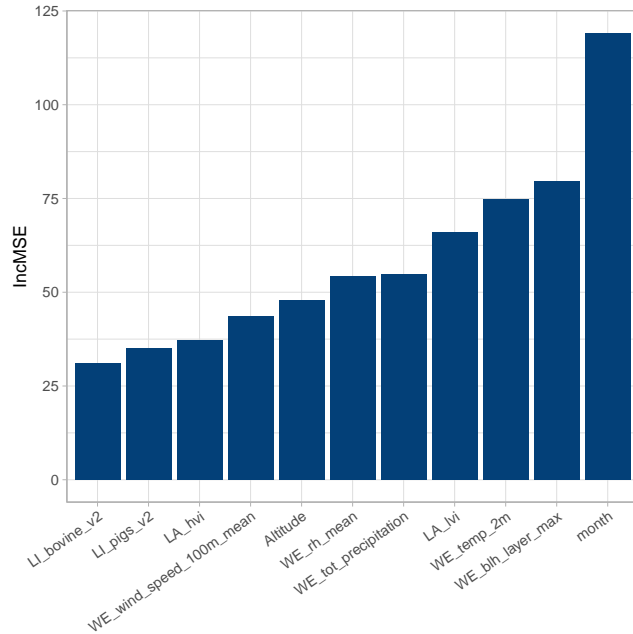


Figure 9: Variable Importance Factor (measured as IncMSE) for the 11 selected features in the large-scale component of the RFSTK.

included (weather) regressors, as we can see by the high importance of the monthly effects. The most important variables after the month are the height of the boundary layer, the temperature and the (low) vegetation index. The bovine density is the least important variable, and indeed, it was not significantly different from zero for the other two models.

For the RFSTK, the spatiotemporal dependence is captured by considering a spatiotemporal Gaussian process with a separable exponential covariance function for space and time. The corresponding variogram model is fitted to the RF residuals. For our analysis, we obtained exponential decay parameters of $\hat{\theta}_{RFSTK_t} = 0.78$ days and $\hat{\theta}_{RFSTK_s} = 0.48^\circ$ for time and space, respectively, the latter corresponds to approximately 50 km. The spatial range parameters are smaller than HDGM because the large scale (RF) explains more variation than the linear large-scale term of HDGM, as shown in Tab. 2.

4.5 Model comparison

Intriguing observations arise when comparing the results of the three models. First, the temporal variation plays an essential role in all three models, as evidenced by the magnitude of the temporal dummy coefficients in HDGM and GAMM (with January as the worst month for air

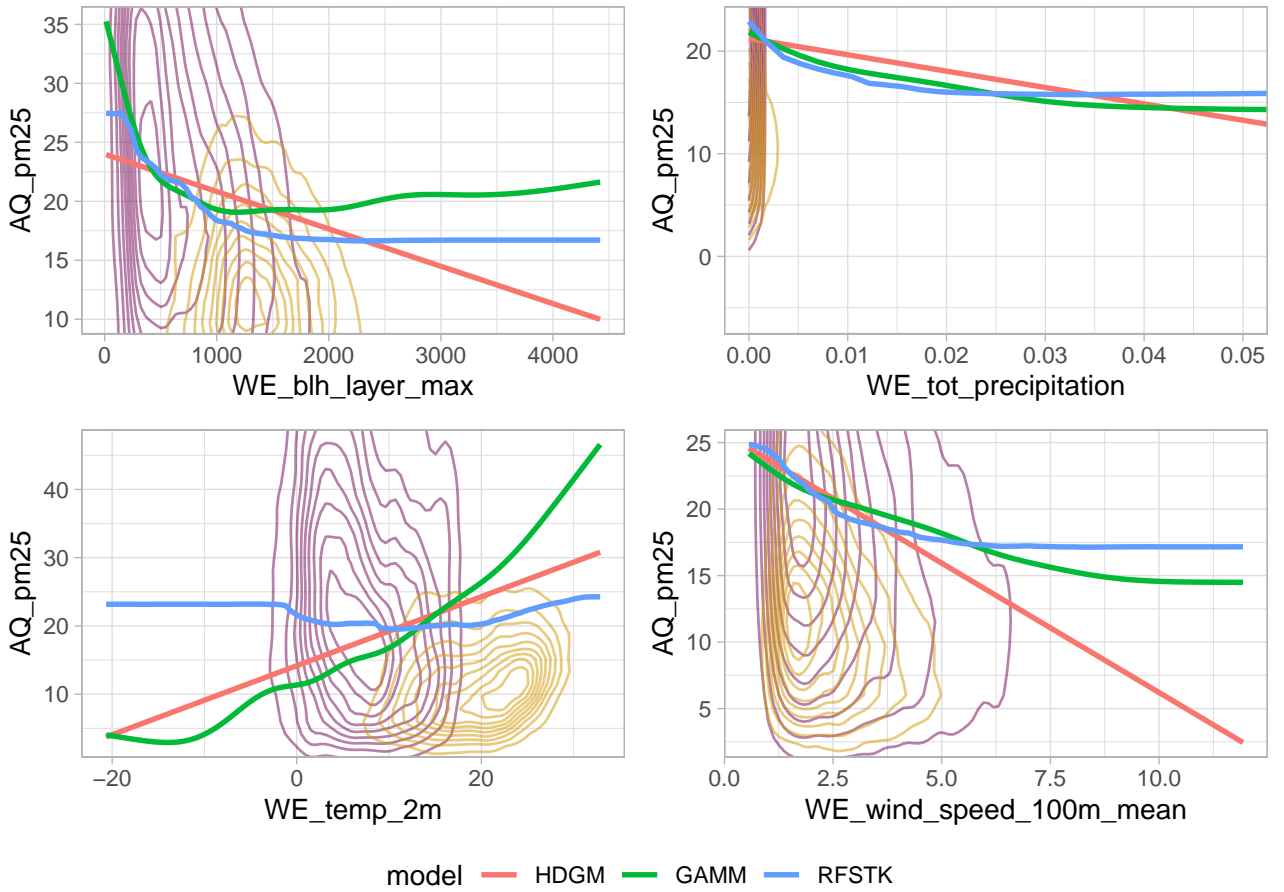


Figure 10: PDP calculated on the large-scale of all three models. Contour lines represent kernel density estimation of the couple ($PM_{2.5}$, $WE_{regressor}$), in yellow for hot months and purple for cold months.

quality) and ‘month’ receiving the highest ranking in the VIF of RFSTK. This suggests that weather variables alone are insufficient for capturing all seasonal variability, even considering the most important weather variables. Interestingly, temperature, which is usually negatively associated with $PM_{2.5}$, was found to be positively related to $PM_{2.5}$ conditional on the month. This is due to the opposing effect of temperature and monthly indicator variables. Furthermore, surprisingly, the significance tests in both HDGM and GAMM on livestock densities suggested that bovine livestock density is not related to $PM_{2.5}$ concentrations, while pig density is.

In Figure 10, we depict partial dependence plots (PDPs) (Friedman, 2001) for selected covariates of all three models along with two-dimensional kernel density estimates of the pairs of $PM_{2.5}$ concentrations and the corresponding regressors in the hot (summer and spring) and cold (autumn and winter) months as yellow and purple contours, respectively. PDPs allow

us to compare the relationships identified within the large-scale of each model and highlight the transition from linear to more complicated relationships. Contrary to the marginal effects, these PDPs account for the typical range of the other predictors. This is accomplished by associating a fixed value of a regressor across all observations with the mean of predicted $\text{PM}_{2.5}$ concentrations. The mean of prediction is calculated for different fixed values of the regressor, typically moving from the minimum to the maximum on an equidistant grid. In other words, PDPs show how the predicted outcome of the changes as a single predictor variable is varied while all other variables are held constant.

It is worth noting that all three models demonstrate similar trends, even though they have different levels of flexibility. For example, they all show that $\text{PM}_{2.5}$ concentrations are higher in cold periods. However, slight differences exist in the models' behaviour, especially for temperature. This suggests there may be nonlinear influences or interactions between temperature and other variables. For example, temperature may have a different impact on $\text{PM}_{2.5}$ concentrations in different altitudes or seasons. RFSTK can capture these interactions more effectively than the other two models, which is why its PDP is flatter. This suggests that RFSTK is better at capturing the complex relationships between $\text{PM}_{2.5}$ concentrations and other variables.

This finding has important implications for the development of air quality models. It suggests that machine learning (ML) techniques can be used to improve the performance and interpretability of classic geostatistical approaches, such as HDGM or GAMM. This is because ML techniques can identify nonlinearities and interactions that are difficult to identify using traditional methods. In the second step, the more interpretable models could include the nonlinear effects and interactions, e.g. GAMM. The comparison of PDPs also highlights the complementary nature of ML techniques and classic approaches. ML techniques are better at capturing complex relationships, while traditional approaches are easier to interpret and allow for straightforward uncertainty estimation. Thus, we advertise combining ML techniques and classic approaches for modelling and predicting PM concentrations.

5 Conclusion

This study compares three statistical models to model and predict Lombardy’s daily $\text{PM}_{2.5}$ concentrations and simultaneously provide an intuitive interpretation of the influencing factors. The models considered are HDGM, GAMM and RFSTK. All three models used are designed to handle spatiotemporal data, although each employs different methods to model external factors and spatiotemporal dependence. The models can generally be divided into large-scale components, small-scale spatiotemporal effects, and measurement and modelling errors. The large-scale components account for external influences, whereas the small-scale components model the spatiotemporal correlation, and the modelling errors contain the unexplained variation of the process.

The large-scale component of the three models showed significant monthly fixed effects for all three models, with negative coefficients for all months. As expected, January was confirmed to be the month with the worst air quality. Furthermore, we used partial dependence plots to compare relationships within the large-scale of the three models and highlight the transition from linear to more complex relationships. The generalised additive mixed model and the random forest approach exhibit similar patterns as they can handle nonlinear relationships. The geostatistical model is constrained by its linear specification, which fits in areas with sufficiently many observations of the covariates. At the same time, linear specification prevents making unreliable predictions – even in regions with few observations for the model estimation. Thus, the hidden dynamic geostatistical showed the best performances in the cross-validation study with an average RMSE of $6.31 \mu\text{g}/\text{m}^3$.

By comparing marginal effects, it is possible to better understand potential interactions and nonlinearities, thereby improving the model’s specification. Indeed, the HDGM can produce good results due to its ability to incorporate latent variables. Still, at the same level of predictive performances, it is preferable to have a model that explains more on a large scale, extending the degree of interpretability. Thus, it can be highly beneficial to detect nonlinear behaviours or interactions by machine learning, which can then be used to improve the specification of the “simpler” but faster model integrated with a more efficient spatiotemporal correlation structure. ML techniques and classic statistical models can be used in complementary ways.

The comparison of models in the field of air quality highlighted that the spatiotemporal

correlation is a crucial aspect that requires careful consideration. However, this correlation is also very sensitive. If not handled properly, it can lead to overfitting the model to the specific data used, thereby hindering its ability to generalise the discovered relations. This limitation was illustrated by the discrepancy in the performance of the HDGM model when evaluated on the entire data set versus when assessed using the leave-one-station-out cross-validation approach.

In conclusion, our findings suggest that classic approaches, such as the hidden dynamic geostatistical model, yield the best predictive performance while being computationally efficient. However, more complex algorithms like random forest can enhance the identification of nonlinear and interaction effects. Therefore, these methods can be used complementary, ushering in a new era where newly developed techniques support traditional and well-established practices.

6 Acknowledgement

This research was funded by Fondazione Cariplo under the grant 2020–4066 “AgrImOnIA: the impact of agriculture on air quality and the COVID-19 pandemic” from the “Data Science for science and society” program.

References

- Baayen, H., Vasishth, S., Kliegl, R., and Bates, D. (2017). The cave of shadows: Addressing the human factor with generalized additive mixed models. *Journal of Memory and Language*, 94:206–234.
- Bai, L., Liu, Z., and Wang, J. (2022). Novel hybrid extreme learning machine and multi-objective optimization algorithm for air pollution prediction. *Applied Mathematical Modelling*, 106:177–198.
- Belgiu, M. and Drăguț, L. (2016). Random forest in remote sensing: A review of applications and future directions. *ISPRS journal of photogrammetry and remote sensing*, 114:24–31.
- Berrocal, V. J., Guan, Y., Muyskens, A., Wang, H., Reich, B. J., Mulholland, J. A., and Chang,

- H. H. (2020). A comparison of statistical and machine learning methods for creating national daily maps of ambient PM_{2.5} concentration. *Atmospheric Environment*, 222:117130.
- Bertaccini, P., Dukic, V., and Ignaccolo, R. (2012). Modeling the short-term effect of traffic and meteorology on air pollution in turin with generalized additive models. *Advances in Meteorology*, 2012.
- Bonas, M. and Castruccio, S. (2021). Calibration of spatio-temporal forecasts from citizen science urban air pollution data with sparse recurrent neural networks. *arXiv preprint arXiv:2105.02971*.
- Bono, R., Alarcón, R., and Blanca, M. J. (2021). Report quality of generalized linear mixed models in psychology: A systematic review. *Frontiers in psychology*, 12:666182.
- Breiman, L. (2001). Random forests. *Machine learning*, 45:5–32.
- Calculi, C., Fassò, A., Finazzi, F., Pollice, A., and Turnone, A. (2015). Maximum likelihood estimation of the multivariate Hidden Dynamic Geostatistical Model with application to air quality in Apulia, Italy. *Environmetrics*, 26(6):406–417.
- Cameletti, M., Ignaccolo, R., and Bande, S. (2011). Comparing spatio-temporal models for particulate matter in Piemonte. *Environmetrics*, 22(8):985–996.
- Cameletti, M., Lindgren, F., Simpson, D., and Rue, H. (2013). Spatio-temporal modeling of particulate matter concentration through the SPDE approach. *AStA Advances in Statistical Analysis*, 97:109–131.
- Chang, L. and Zou, T. (2022). Spatio-temporal analysis of air pollution in North China Plain. *Environmental and Ecological Statistics*, 29(2):271–293.
- Chen, L., Wang, Y., Ren, C., Zhang, B., and Wang, Z. (2019). Assessment of multi-wavelength SAR and multispectral instrument data for forest aboveground biomass mapping using random forest kriging. *Forest ecology and management*, 447:12–25.
- Cressie, N. and Wikle, C. K. (2015). *Statistics for spatio-temporal data*. John Wiley & Sons.
- Daw, R. and Wikle, C. K. (2023). REDS: random ensemble deep spatial prediction. *Environmetrics*, 34(1):e2780.

- Ding, C., Wang, G., Zhang, X., Liu, Q., and Liu, X. (2021). A hybrid CNN-LSTM model for predicting PM_{2.5} in Beijing based on spatiotemporal correlation. *Environmental and Ecological Statistics*, 28(3):503–522.
- European Environmental Agency (2022a). Air quality in Europe. Last Access: 18-03-2023.
- European Environmental Agency (2022b). Classification of monitoring stations and criteria to include them in EEA’s assessments products. https://www.eea.europa.eu/ds_resolveuid/cb32af951deb4e40aef444bdd37d9306 [Accessed: (2023-03-12)].
- Fahrmeir, L., Kneib, T., and Lang, S. (2004). Penalized structured additive regression for space-time data: a Bayesian perspective. *Statistica Sinica*, pages 731–761.
- Fahrmeir, L. and Lang, S. (2001). Bayesian inference for generalized additive mixed models based on Markov random field priors. *Journal of the Royal Statistical Society Series C: Applied Statistics*, 50(2):201–220.
- Fasiolo, M., Nedellec, R., Goude, Y., and Wood, S. N. (2020). Scalable visualization methods for modern generalized additive models. *Journal of Computational and Graphical Statistics*, 29(1):78–86.
- Fassò, A. and Finazzi, F. (2011). Maximum likelihood estimation of the dynamic coregionalization model with heterotopic data. *Environmetrics*, 22(6):735–748.
- Fassò, A., Maranzano, P., and Otto, P. (2022). Spatiotemporal variable selection and air quality impact assessment of COVID-19 lockdown. *Spatial Statistics*, 49:100549.
- Fassò, A., Rodeschini, J., Fusta Moro, A., Shaboviq, Q., Maranzano, P., Cameletti, M., Finazzi, F., Golini, N., Ignaccolo, R., and Otto, P. (2023). Agrimonia: a dataset on livestock, meteorology and air quality in the Lombardy region, Italy. *Scientific Data*.
- Fassò, A., Rodeschini, J., Fusta Moro, A., Shaboviq, Q., Maranzano, P., Cameletti, M., Finazzi, F., Golini, N., Ignaccolo, R., and Otto, P. (2023). AgrImOnIA: Open Access dataset correlating livestock and air quality in the Lombardy region, Italy.
- Finazzi, F., Scott, E. M., and Fassò, A. (2013). A model-based framework for air quality indices and population risk evaluation, with an application to the analysis of scottish air quality data. *Journal of the Royal Statistical Society. Series C, Applied Statistics*, 62(2):287.

- Fioravanti, G., Martino, S., Cameletti, M., and Cattani, G. (2021). Spatio-temporal modelling of PM₁₀ daily concentrations in Italy using the SPDE approach. *Atmospheric Environment*, 248:118192.
- Fox, E. W., Ver Hoef, J. M., and Olsen, A. R. (2020). Comparing spatial regression to random forests for large environmental data sets. *PloS one*, 15(3):e0229509.
- Friedman, J. H. (2001). Greedy function approximation: a gradient boosting machine. *Annals of statistics*, pages 1189–1232.
- Fusta Moro, A., Salis, M., Andrea, Z., Michela, C., Golini, N., Ignaccolo, R., et al. (2022). Ammonia emissions and fine particulate matter: some evidence in Lombardy. In *Book of Short Papers of the ASA Conference 2022-Data-Drive Decision Making*, pages 1–6.
- Grange, S. K., Sintermann, J., and Hueglin, C. (2023). Meteorologically normalised long-term trends of atmospheric ammonia (NH₃) in Switzerland/Liechtenstein and the explanatory role of gas-aerosol partitioning. *Science of the Total Environment*, page 165844.
- Gräler, B., Pebesma, E., and Heuvelink, G. (2016). Spatio-temporal interpolation using gstat. *The R Journal*, 8:204–218.
- Guo, P.-T., Li, M.-F., Luo, W., Tang, Q.-F., Liu, Z.-W., and Lin, Z.-M. (2015). Digital mapping of soil organic matter for rubber plantation at regional scale: An application of random forest plus residuals kriging approach. *Geoderma*, 237:49–59.
- Handcock, M. S. and Wallis, J. R. (1994). An approach to statistical spatial-temporal modeling of meteorological fields. *Journal of the American Statistical Association*, 89(426):368–378.
- Hastie, T. and Tibshirani, R. (1987). Generalized additive models: some applications. *Journal of the American Statistical Association*, 82(398):371–386.
- Huang, H.-C. and Cressie, N. (1996). Spatio-temporal prediction of snow water equivalent using the Kalman filter. *Computational Statistics & Data Analysis*, 22(2):159–175.
- Ignaccolo, R., Mateu, J., and Giraldo, R. (2014). Kriging with external drift for functional data for air quality monitoring. *Stochastic environmental research and risk assessment*, 28:1171–1186.

- Jato-Espino, D. and Mayor-Vitoria, F. (2023). A statistical and machine learning methodology to model rural depopulation risk and explore its attenuation through agricultural land use management. *Applied Geography*, 152:102870.
- Javanmard, M. E. and Ghaderi, S. (2022). A hybrid model with applying machine learning algorithms and optimization model to forecast greenhouse gas emissions with energy market data. *Sustainable Cities and Society*, 82:103886.
- Jerrett, M., Arain, A., Kanaroglou, P., Beckerman, B., Potoglou, D., Sahuvaroglu, T., Morrison, J., and Giovis, C. (2005). A review and evaluation of intraurban air pollution exposure models. *Journal of Exposure Science & Environmental Epidemiology*, 15(2):185–204.
- Jiang, J. and Nguyen, T. (2007). *Linear and generalized linear mixed models and their applications*, volume 1. Springer.
- Jui, S. J. J., Ahmed, A. M., Bose, A., Raj, N., Sharma, E., Soar, J., and Chowdhury, M. W. I. (2022). Spatiotemporal hybrid random forest model for tea yield prediction using satellite-derived variables. *Remote Sensing*, 14(3):805.
- Kammann, E. and Wand, M. P. (2003). Geoaddivitive models. *Journal of the Royal Statistical Society: Series C (Applied Statistics)*, 52(1):1–18.
- Kishi, S., Sun, J., Kawaguchi, A., Ochi, S., Yoshida, M., and Yamanaka, T. (2023). Characteristic features of statistical models and machine learning methods derived from pest and disease monitoring datasets. *Royal Society Open Science*, 10(6):230079.
- Knape, J. (2016). Decomposing trends in Swedish bird populations using generalized additive mixed models. *Journal of Applied Ecology*, 53(6):1852–1861.
- Kneib, T., Knauer, F., and Küchenhoff, H. (2011). A general approach to the analysis of habitat selection. *Environmental and Ecological Statistics*, 18:1–25.
- Kulkarni, P., Sreekanth, V., Upadhyaya, A. R., and Gautam, H. C. (2022). Which model to choose? Performance comparison of statistical and machine learning models in predicting PM_{2.5} from high-resolution satellite aerosol optical depth. *Atmospheric Environment*, 282:119164.

- Liaw, A. and Wiener, M. (2002). Classification and regression by randomforest. *R News*, 2(3):18–22.
- Liu, Y., Cao, G., Zhao, N., Mulligan, K., and Ye, X. (2018). Improve ground-level PM_{2.5} concentration mapping using a random forests-based geostatistical approach. *Environmental pollution*, 235:272–282.
- Liu, Y., Zhao, N., Vanos, J. K., and Cao, G. (2019). Revisiting the estimations of PM_{2.5}-attributable mortality with advancements in PM_{2.5} mapping and mortality statistics. *Science of the Total Environment*, 666:499–507.
- Lovarelli, D., Conti, C., Finzi, A., Bacenetti, J., and Guarino, M. (2020). Describing the trend of ammonia, particulate matter and nitrogen oxides: The role of livestock activities in northern Italy during Covid-19 quarantine. *Environmental research*, 191:110048.
- Lu, M., Cavieres, J., and Moraga, P. (2023). A comparison of spatial and nonspatial methods in statistical modeling of NO₂: Prediction accuracy, uncertainty quantification, and model interpretation. *Geographical Analysis*.
- Maranzano, P., Otto, P., and Fassò, A. (2023). Adaptive LASSO estimation for functional hidden dynamic geostatistical models. *Stochastic Environmental Research and Risk Assessment*, pages 1–23.
- Maranzano, P. and Pelagatti, M. (2023). Spatiotemporal event studies for environmental data under cross-sectional dependence: An application to air quality assessment in lombardy. *Journal of Agricultural, Biological and Environmental Statistics*, pages 1–22.
- Merk, M. S. and Otto, P. (2020). Estimation of anisotropic, time-varying spatial spillovers of fine particulate matter due to wind direction. *Geographical Analysis*, 52(2):254–277.
- Meyer, H., Reudenbach, C., Hengl, T., Katurji, M., and Nauss, T. (2018). Improving performance of spatio-temporal machine learning models using forward feature selection and target-oriented validation. *Environmental Modelling & Software*, 101:1–9.
- Nag, P., Sun, Y., and Reich, B. J. (2023). Spatio-temporal DeepKriging for interpolation and probabilistic forecasting. *Spatial Statistics*, page 100773.

- Najafabadi, A. M., Mahaki, B., and Hajizadeh, Y. (2020). Spatiotemporal modeling of airborne fine particulate matter distribution in Isfahan. *International Journal of Environmental Health Engineering*, 9(July):1–7.
- Nowak, G. and Welsh, A. (2020). Improved prediction for a spatio-temporal model. *Environmental and Ecological Statistics*, 27:631–648.
- Otto, P., Doğan, O., and Taşpınar, S. (2022). A dynamic spatiotemporal stochastic volatility model with an application to environmental risks. *arXiv preprint arXiv:2211.03178*.
- Otto, P., Piter, A., and Gijsman, R. (2021). Statistical analysis of beach profiles—A spatiotemporal functional approach. *Coastal engineering*, 170:103999.
- Patelli, L., Cameletti, M., Golini, N., and Ignaccolo, R. (2023). A path in regression random forest looking for spatial dependence: a taxonomy and a systematic review.
- Pernigotti, D., Georgieva, E., Thunis, P., and Bessagnet, B. (2012). Impact of meteorological modelling on air quality: Summer and winter episodes in the Po valley (Northern Italy). *International Journal of Environment and Pollution*, 50(1-4):111–119.
- Piter, A., Otto, P., and Alkhatib, H. (2022). The Helsinki bike-sharing system—insights gained from a spatiotemporal functional model. *Journal of the Royal Statistical Society Series A: Statistics in Society*, 185(3):1294–1318.
- Qi, Y. (2012). Random forest for bioinformatics. *Ensemble machine learning: Methods and applications*, pages 307–323.
- Sekulić, A., Kilibarda, M., Heuvelink, G. B., Nikolić, M., and Bajat, B. (2020). Random forest spatial interpolation. *Remote Sensing*, 12(10):1687.
- Shao, Y., Ma, Z., Wang, J., and Bi, J. (2020). Estimating daily ground-level PM_{2.5} in China with random-forest-based spatiotemporal kriging. *Science of The Total Environment*, 740:139761.
- Stafoggia, M., Bellander, T., Bucci, S., Davoli, M., De Hoogh, K., De’Donato, F., Gariazzo, C., Lyapustin, A., Michelozzi, P., Renzi, M., et al. (2019). Estimation of daily PM₁₀ and PM_{2.5} concentrations in Italy, 2013–2015, using a spatiotemporal land-use random-forest model. *Environment international*, 124:170–179.

- Sun, W. and Xu, Z. (2022). A hybrid daily PM_{2.5} concentration prediction model based on secondary decomposition algorithm, mode recombination technique and deep learning. *Stochastic Environmental Research and Risk Assessment*, pages 1–20.
- Taghavi-Shahri, S. M., Fassò, A., Mahaki, B., and Amini, H. (2020). Concurrent spatiotemporal daily land use regression modeling and missing data imputation of fine particulate matter using distributed space-time expectation maximization. *Atmospheric environment*, 224:117202.
- Thunis, P., Clappier, A., Beekmann, M., Putaud, J. P., Cuvelier, C., Madrazo, J., and de Meij, A. (2021). Non-linear response of PM_{2.5} to changes in NO_x and NH₃ emissions in the Po Basin (Italy): consequences for air quality plans. *Atmos. Chem. Phys.*, 21(12):9309–9327.
- Tsokov, S., Lazarova, M., and Aleksieva-Petrova, A. (2022). A hybrid spatiotemporal deep model based on CNN and LSTM for air pollution prediction. *Sustainability*, 14(9):5104.
- Viscarra Rossel, R. A., Webster, R., and Kidd, D. (2014). Mapping gamma radiation and its uncertainty from weathering products in a Tasmanian landscape with a proximal sensor and random forest kriging. *Earth Surface Processes and Landforms*, 39(6):735–748.
- Wang, L., Wu, W., and Liu, H.-B. (2019). Digital mapping of topsoil ph by random forest with residual kriging (RFRK) in a hilly region. *Soil Research*, 57(4):387–396.
- Wang, Y., Finazzi, F., and Fassò, A. (2021). D-STEM v2: a software for modeling functional spatio-temporal data. *Journal of Statistical Software*, 99:1–29.
- WHO (2021). WHO global air quality guidelines: particulate matter (PM_{2.5} and PM₁₀), ozone, nitrogen dioxide, sulfur dioxide and carbon monoxide: executive summary.
- Wilkinson, G. N. and Rogers, C. E. (1973). Symbolic description of factorial models for analysis of variance. *Journal of the Royal Statistical Society. Series C (Applied Statistics)*, 22(3):392–399.
- Wood, S. N. (2011). Fast stable restricted maximum likelihood and marginal likelihood estimation of semiparametric generalized linear models. *Journal of the Royal Statistical Society (B)*, 73(1):3–36.

- Wood, S. N. (2017). *Generalized additive models: an introduction with R*. Chapman and Hall/CRC.
- Zhan, Y., Luo, Y., Deng, X., Zhang, K., Zhang, M., Grieneisen, M. L., and Di, B. (2018). Satellite-based estimates of daily NO₂ exposure in China using hybrid random forest and spatiotemporal kriging model. *Environmental science & technology*, 52(7):4180–4189.
- Zhang, L., Cheng, Y., Zhang, Y., He, Y., Gu, Z., Yu, C., et al. (2017). Impact of air humidity fluctuation on the rise of PM mass concentration based on the high-resolution monitoring data. *Aerosol and Air Quality Research*, 17(2):543–552.